An Ising-like Model to Predict Dielectric Properties of the Relaxor Ferroelectric Solid Solution $BaTiO_3 - Bi(Zn_{1/2}Ti_{1/2})O_3$

Dennis L. Jackson and David Roundy
Department of Physics, Oregon State University, Corvallis, OR 97331

We model the dielectric properties of the relaxor ferroelectric perovskite solid solution $BaTiO_3$ - $Bi(Zn_{1/2}Ti_{1/2})O_3$ (BT-BZT) using *ab initio* methods combined with an Ising-like model. BT-BZT has both A-site and B-site disorder, which makes it a challenging material to model. The polarization of all possible $2 \times 2 \times 2$ supercells of BT-BZT are determined using *ab initio* methods. The cells are then arranged on a lattice in an Ising-like model to determine long-range dielectric properties. This enables us to predict the long-range disorder effects of relaxors, while keeping the accuracy of *ab initio* methods. This new model enables us to work with orders of magnitude more atoms than other models such as molecular dynamics. We analyze the Monte Carlo data for a single lattice configuration using the multiple histogram method, and develop a new modified histogram technique to combine data from multiple lattice configurations. Experiments qualitatively agree with our models predicted values of dielectric constant and polarization.

I. INTRODUCTION

Relaxor ferroelectrics (commonly known as relaxors) feature a broad maximum of their dielectric permittivity, and a strong frequency dependence of the temperature at which that maximum occurs. Relaxors have been the subject of considerable research[1–8], due to their fundamental scientific interest, as well as their use in technological applications such as capacitors and piezoelectric devices[9].

Burns and Dacol[10] first ascribed the diffuse phase transition seen in relaxors to the formation of polar nano-regions (PNR) below the so-called Burns temperature (T_b). The PNRs consist of groups of correlated dipoles, which explains the anomalous relaxation times observed in the frequency-dependent dielectric response. The PNRs generally appear as a result of compositional disorder[11? –13], which poses a challenge to model effectively. There have been many attempts with varying levels of success. These methods include molecular dynamics (MD) simulations[14–17], density functional theory (DFT) calculations[18–20], spherical random-bond-random-field model[21], random field-Ising-models[22,23], other Monte Carlo (MC) simulations[24]. For a good summary of many of these methods applied to relaxors, see Burton et. al.[18]. While DFT calculations are quite accurate, they are limited to small supercells of no more than a few dozen atoms. MD calculations are able to observe a few thousand atoms before the computational demands become too great. MC simulations are able to model enough atoms to capture the long-range disorder effects needed to describe relaxors, but do not have the accuracy of *ab initio* methods. We aim to create a model using both DFT and a MC Ising-like method to try and capture the accuracy of DFT, while utilizing the long-range scaling of Ising models.

In this paper, we study the $x\mathrm{BaTiO_3} + (1 - x)\mathrm{Bi(Zn_{1/2}Ti_{1/2})O_3}$ solid solution (BT-BZT), which has been recently studied and found to exhibit relaxor behavior, with a striking peak value of permittivity[25–27]. Unlike many relaxor ferroelectrics, BT-BZT exhibits disorder in both the A-site and the B-site. Experimentally, BT-BZT is found to be slightly tetragonal for compositions containing mostly BT, with a c/a ratio of approximately 1.01 as an upper limit[25]. Experiments also show that as the composition of BT-BZT contains less BT, the sharp ferroelectric phase transition is lost, and the solid solution transitions to relaxor behavior[25,27].

II. MODEL

We model this relaxor behavior by using a combination of techniques including *ab initio* methods and an Ising-like model. The *ab initio* calculations are accurate at small length scales, but lack the ability to describe long-range interactions. The Ising-like model is able describe long-range effects, but cannot predict short-range interactions. By combining these methods into a single model we gain insight into the larger picture by including both long and short-range effects.

Our *ab initio* calculations are restricted to $2 \times 2 \times 2$ supercells of BT-BZT for symmetry. This allows for compositions of $x = 0, 0.25, 0.5, 0.75, 1$, in the 40 atom supercell. Table I shows the number of distinct configurations for each composition, and Figure 1 shows one possible atomic configuration for a $2 \times 2 \times 2$ supercell with a single zinc atom ($x = 0.75$). With the Quantum Espresso[28] package we use Density Functional Theory (DFT) and the Modern Theory of Polarization (MTP)[29–31] to determine the energies and polarizations of each unique configuration. The DFT calculations were run using a PBE-GGA exchange-correlation functional, ultrasoft pseudopotentials, a cutoff energy of 80 Rydberg, and a $2 \times 2 \times 2$ Monkhorst-Pack k-point grid.

The polarizations determined by MTP are not unique for each cell. The actual polarization is only accurate modulo $e\vec{R}/\Omega$, where e is the charge of an electron, $\vec{R}$ is a lattice vector, and Ω is the cell volume. We are able to determine the polarization of the relaxed cell relative

to the polarization of a cell with atoms in the symmetric positions. Some configurations may also have degenerate polarization states. For cells with more than one polarization, all accessible states are recorded and used later in the Monte Carlo simulations.

There are some disadvantages to using *ab initio* methods to model relaxors. Most importantly, relaxors display long-range disorder, which is not efficiently modeled using *ab initio* techniques. By using a lattice model, we are able to observe some long-range effects, as well as study any compositional value x.

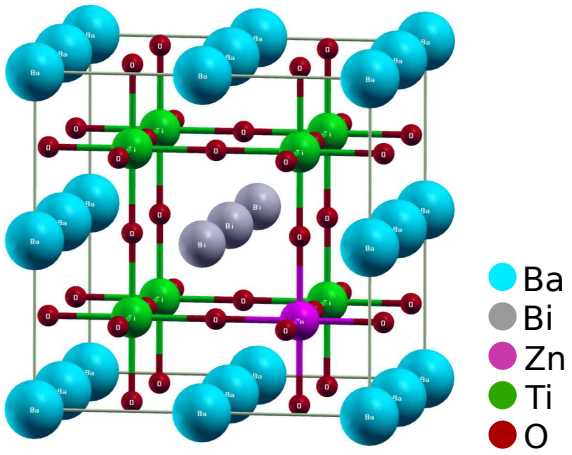

FIG. 1: (color online) BT-BZT cubic $2 \times 2 \times 2$ supercell example with $x = 0.75$. The lattice constant of the supercell is twice that of the smallest cubic BT unit cell.

TABLE I: The number of unique atomic configurations for each composition of a $2 \times 2 \times 2$ supercell.

Number of Zn atoms	Composition x	Distinct configurations
0	1.0	1
1	0.75	3
2	0.50	26
3	0.25	13
4	0.0	6

Once we have determined the energies and all polarization states of each configuration for all compositions, we are able use this data as the basis of an Ising-like model. The classic Ising model is used to determine critical behavior for ferromagnetic systems on a lattice, where each lattice may have a spin up/down state[32–34]. An extension of the Ising model is the Heisenberg model which may have spins in any direction. Here, we create a lattice of our $2 \times 2 \times 2$ supercells and use only the polarizations determined by the MTP calculations. This differs from both Ising and Heisenberg models in that the polarizations are not simple up and down, but neither are they allowed to point in any direction. This adaptation is not unlike a Potts model[35–37] in that there are discrete directions of the polarizations, but our polarizations are not uniform in nature and each cell on the lattice may have different accessible polarization states. We use the interaction Hamiltonian of the Heisenberg model

$$H = -\frac{J}{2} \sum_{i}^{cells} \sum_{j}^{NN} \vec{p}_i \cdot \vec{p}_j - \sum_{i}^{cells} \vec{p}_i \cdot \vec{E} \,, \tag{1}$$

where $\vec{p}_i$ is the polarization of a single cell, $\vec{E}$ is the external electric field and J is a coupling constant. The coupling constant is tuned to match the experimental Curie temperature of pure barium titanate using the fourth order Binder cumulant method[38].

Using the energies and polarizations from the *ab initio* calculations, we populate a lattice of cells to obtain the desired composition x. The number of each unique $2\times2\times2$ cells is determined using Boltzmann statistics, and the cells are distributed on the lattice stochastically. Once the lattice is established, we begin with the Monte Carlo simulation.

For each desired temperature and composition, we equilibrate for at least 10^6 flips per cell. The total polarization and energy are recorded after every 10 changes per site. Equilibrium is considered to be reached when the system has run for several energy correlation times. Once the system has reached equilibrium, we can calculate the mean value of any function of the energy and polarization simply by

$$\langle f(E, \vec{p}) \rangle = \frac{1}{N} \sum_{i=1}^{N} f(E_i, \vec{p}_i) \,, \tag{2}$$

where the subscript i is the index of a particular data sample, and N is the total number of samples. We can then calculate properties such as the dielectric constant and specific heat using the variance of the polarization and energy respectively.

Unfortunately, we need to run a separate simulation for each temperature and composition. By using the histogram method, a single simulation can be used to determine results near the simulation temperature[39]. This idea is expanded to use simulation data at multiple temperatures to determine results for a large range of temperatures.

The multiple histogram equations are given by

$$\tilde{P}_\beta(E, \vec{p}) = \frac{\sum_{n=1}^{N} H_n(E, \vec{p}) g_n^{-1} \exp\left(-\beta E\right)}{\sum_{m=1}^{N} n_m g_m^{-1} \exp\left(-\beta_m E - f_m\right)} \,, \tag{3}$$

where $\beta_m = 1/k_B T_m$, N is the number of simulations, $H_n(E, \vec{p})$ is the histogram of the n^{th} simulation, n_m is the total number of samples included in the m^{th} histogram, $g_n = 1 + 2\tau_n$ where τ_n is the correlation time, and f_m is an estimate of the dimensionless free energy of the m^{th} simulation. The correlation time is incorporated as a weighting factor to account for the differing correlation times of the samples for different simulations. The free energies serve as a correction factor due to combining

data from multiple temperatures, and are calculated self consistently using

$$\exp\left(f_m\right) = \tilde{P}_{\beta_m}(E,\vec{p}) \ . \tag{4}$$

Note that Equation 3 does not give the actual probability, but a probability distribution function that must be normalized:

$$P_\beta(E,\vec{p}) = \frac{\tilde{P}_\beta(E,\vec{p})}{\sum_{E,\vec{p}} \tilde{P}_\beta(E,\vec{p})} \ . \tag{5}$$

Once the probabilities are determined, we are able to calculate the mean value of a quantity using

$$\langle f(E,\vec{p})\rangle_\beta = \sum_i^{N_E} \sum_j^{N_p} f(E_i,\vec{p}_j) P_\beta(E_i,\vec{p}_j) \ , \tag{6}$$

By calculating the mean of the polarization in a given direction $\langle P_x \rangle$, as well as $\langle {P_x}^2 \rangle$, we can use the variance of the polarization to calculate the susceptibility by

$$\chi_{xx} = \beta \left(\langle {P_x}^2 \rangle - \langle P_x \rangle^2 \right) \ , \tag{7}$$

and the dielectric constant by $\epsilon = 1 + 4\pi\chi$.

Figure 2 compares the dielectric constant for single simulations at every 10 K and the multiple histogram method using the data from the same input simulations. The multiple histogram method can be thought of as an interpolation scheme if there are enough data samples at all of the simulation temperatures.

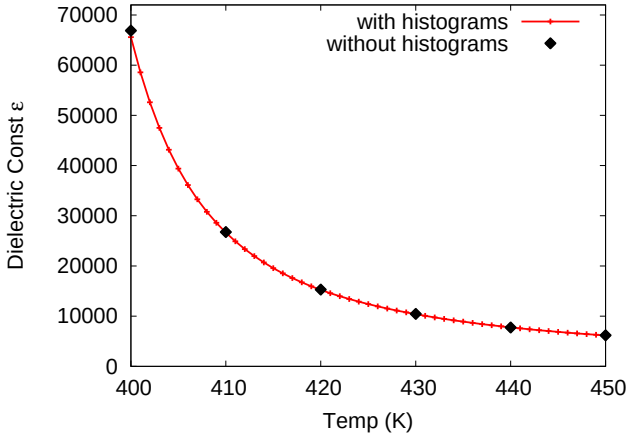

FIG. 2: (color online) Dielectric constant of BT ($x = 1$) on a $16 \times 16 \times 16$ lattice using raw data and the multiple histogram method. The simulations used for the old method are also the inputs in this multiple histogram method. The multiple histogram method is sampled every 1K, while the input simulations were performed every 10K.

A. Combined-Multiple Histogram Method

Since not every cell on the lattice is identical for compositions of $x < 1$, there is more than one way to arrange the cells on the lattice. If we wish to combine the results of multiple arrangements into a single result, we must use an appropriately weighted average. The weighted result must be equivalent to using one large lattice that contains each other lattice as a subset. In order to combine these results we multiply the probabilities and sum over all states with an appropriate Kronecker delta.

$$\begin{aligned} P_{\beta,tot}\left(E,\vec{p}\right) = & \\ \sum_{E_1,\vec{p}_1} \sum_{E_2,\vec{p}_2} \ldots \sum_{E_n,\vec{p}_n} & P_{\beta,1}\left(E_1,\vec{p}_1\right) P_{\beta,2}\left(E_2,\vec{p}_2\right) \times \ldots \\ & \times P_{\beta,N}\left(E_N,\vec{p}_N\right) \times \delta_{E,(E_1+E_2+\ldots+E_N)} \times \\ & \delta_{\vec{p},(\vec{p}_1+\vec{p}_2+\ldots+\vec{p}_N)} \ , \end{aligned} \tag{8}$$

where the subscript β indicates the dependence of probability on temperature. The total probability is a function of the sum of all energies and polarizations. This works on the assumption that the systems are non-interacting and independent. This method is quite expensive computationally, so we utilized convolutions to speed up the calculations. This technique may also be applied to multiple runs of the same configuration, to avoid having to repeat costly calculations. We are also able to use this method to combine polarization data from all cartesian directions into a single weighted value. Figure 3 shows a single cartesian component of the dielectric constant for five different lattice configurations of a single composition, along with the weighted combined result.

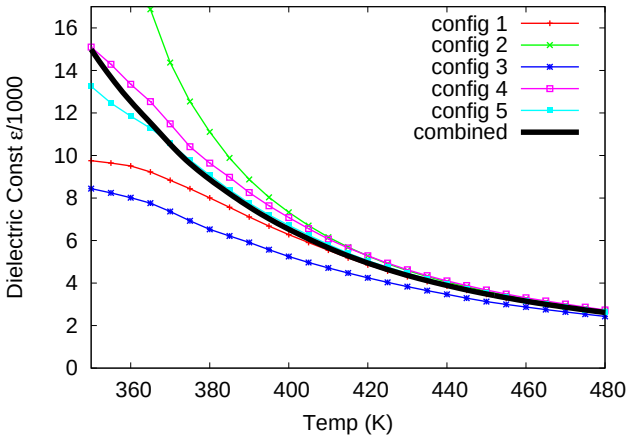

FIG. 3: (color online) The dielectric constant of a single component of the polarization for each of five different lattice configurations and the combined result for $x = 0.95$.

We are able to determine the uncertainty in our calculations with the regular multiple histogram method by first finding the uncertainty in the probabilities:

$$\delta P_\beta\left(E,\vec{p}\right) = \left(\sum_{n=1}^{N} \frac{H_n\left(E,\vec{p}\right)}{g_n} \right)^{-1/2} P_\beta\left(E,\vec{p}\right) \ , \tag{9}$$

where the sum is over all simulations, $H_n(E,\vec{p})$ is the histogram of a single simulation, and $g_n = 1 + 2\tau_n$ is the

correlation time factor[40]. The uncertainty in the total probability of Equation 8 is then given by

$$\delta P_{tot}^2 = \sum_1 \left(\frac{\partial P}{\partial P_1}\delta P_1\right)^2 + \sum_2 \left(\frac{\partial P}{\partial P_2}\delta P_2\right)^2 + ... + \sum_N \left(\frac{\partial P}{\partial P_N}\delta P_N\right)^2 , \quad (10)$$

where the uncertainty for each lattice configuration δP_i is calculated using Equation 9.

The derivative of Equation 8 with respect to a single lattice configuration probability is

$$\frac{\partial P}{\partial P_i} = \sum_1 ... \sum_{i-1} \sum_{i+1} ... \sum_N P_1 ... P_{i-1} P_{i+1} ... P_N \ . \quad (11)$$

The error in the total probability is then given by

$$\delta P_{tot}^2 = \sum_1 \left[(\delta P_1)^2 \left(\sum_2 \sum_3 ... \sum_N P_2 P_3 ... P_N \right)^2 \right] + \sum_2 \left[(\delta P_2)^2 \left(\sum_1 \sum_3 ... \sum_N P_1 P_3 ... P_N \right)^2 \right] + ... + \sum_N \left[(\delta P_N)^2 \left(\sum_1 \sum_2 ... \sum_{N-1} P_1 P_2 ... P_{N-1} \right)^2 \right] . \quad (12)$$

The uncertainties of the susceptibility can be determined using

$$\delta\chi^2 = \sum_{E,\vec{p}} \left(\frac{\partial \chi(\vec{p})}{\partial P_\beta(E,\vec{p})} \delta P_\beta(E,\vec{p}) \right)^2 . \quad (13)$$

By carrying out the derivative, we get

$$\delta\chi^2 = \frac{\beta^2}{Z_\beta^2} \sum_{E,\vec{p}} \left[\left[\vec{p}^{\,2} - \langle \vec{p}^{\,2} \rangle + 2\langle \vec{p} \rangle^2 - 2\langle \vec{p} \rangle \vec{p} \right]^2 (\delta P_\beta(E,\vec{p}))^2 \right] , \quad (14)$$

where

$$Z_\beta = \sum_{E,\vec{p}} P_\beta(E,\vec{p}) \ . \quad (15)$$

III. RESULTS AND DISCUSSION

A. Dielectric Constant

The results of our model are compared with the experiments of Huang and Cann[25], where all of the results produced by the model were found using the combined histogram method. Each combined data set is found using simulations performed on a $16 \times 16 \times 16$ lattice at every 5 Kelvin, each with at least 10^6 Monte Carlo flips per cell.

Figure 4 shows the dielectric constant for the model and experiment for various compositions. Each of the experimental results of the dielectric constant are shown for a range of frequencies. In general, at high temperatures there is little to no frequency dependence of the experimental dielectric constant, while at low temperature there is some frequency dependence that grows larger as the composition decreases. The predicted dielectric constant at low temperatures does not match experiment for any composition, due to the frequency dependence and the fact that our model only predicts the zero-frequency limit.

The top section of Figure 4 shows the dielectric constant for pure barium titanate (BT) ($x = 1$). The experimental results show a clear transition near the Curie temperature of $393K$, and essentially no difference between the various frequencies. The model prediction shows a very precise curve, as the error bars are smaller than the thickness of the line. However, the value of the curve is not as accurate as one could hope. The predicted dielectric constant is well above the experimental value for all temperatures. For temperatures slightly above the critical point, the dielectric constant is almost an order of magnitude too high, and at high temperatures the difference is around a factor of two.

Below the critical point, the predicted value diverges, while the experimental value drops down significantly. This divergence can be understood by considering that the model computes the zero frequency limit (DC) in thermal equilibrium[24].

At low temperatures, a ferroelectric is not likely to change polarizations over short time scales. Thus, only a single polarization state is all that is needed to determine the dielectric properties. The combined histogram method includes many polarization states for each temperature, and thus gives a non-physical result below the critical temperature. One possible solution would be to break the symmetry of the system by calculating the probabilities used to determine the dielectric constant in the presence of a small applied electric field. This would force the system to have only those polar states that are aligned with the electric field. In practice, the symmetry breaking leads to instabilities in both the dielectric constant and specific heat, which is likely due to poor convergence in our low temperature simulations.

The middle section of Figures 4 shows the experimental and model data for $BaTiO_3$ - $Bi(Zn_{1/2}Ti_{1/2})O_3$ (BT-BZT) with a composition of $x = 0.95$. The model data was found using the combined histogram method with the $\hat{x}$, $\hat{y}$, and $\hat{z}$ components of the polarization for five different lattice configurations. This is roughly equivalent to using a single component of the polarization for 15 separate lattice configurations. Since there are multiple configurations being considered, there is a visibly

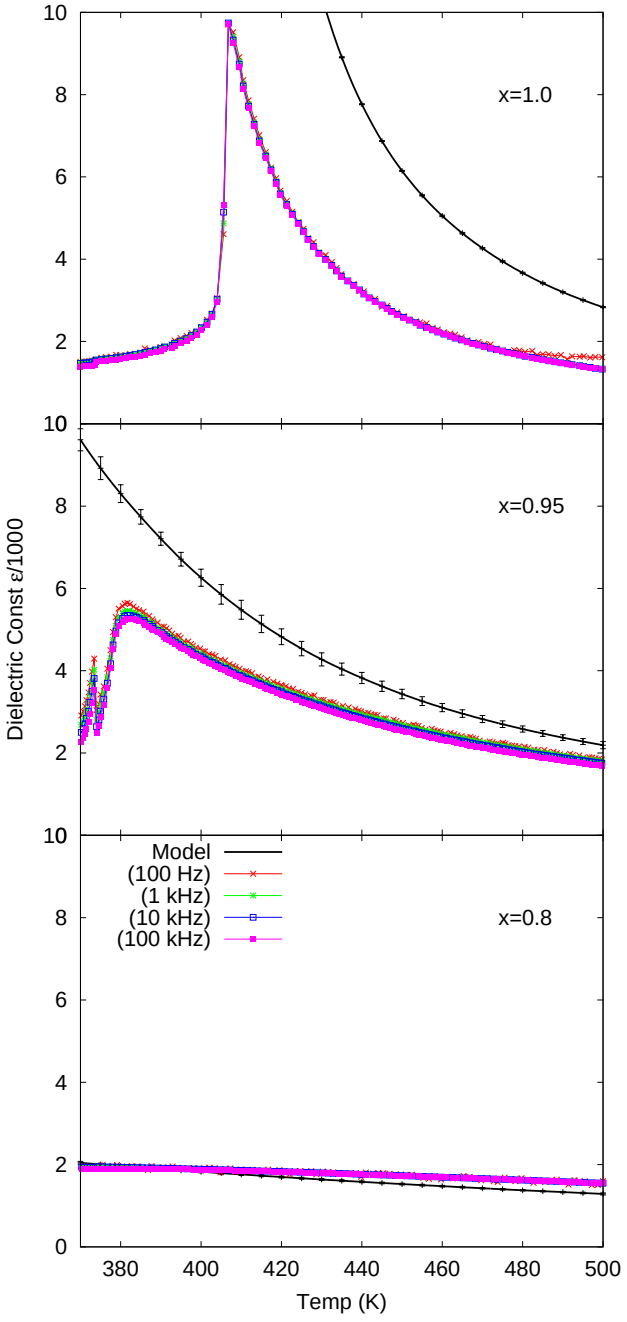

FIG. 4: (color online) The dielectric constant of three compositions, $x = 1$, $x = 0.95$ and $x = 0.8$. The predicted result is compared with experimental measurements made at several frequencies[25]. Theory is in black, with error bars given. Experiment is shown with colored symbols.

larger uncertainty in the dielectric constant for $x = 0.95$ than for pure BT ($x = 1$).

The experimental data for $x = 0.95$ still shows some critical behavior at a slightly lower temperature than pure BT. The model predicts the dielectric constant reasonably well at high temperatures. The difference between the model data and experimental data is now much less than a factor of two, even as the temperature decreases. For lower temperatures the model predictions still diverge for these compositions. The temperature at which this divergence occurs, however, is much lower than that of pure BT.

The lower section of Figures 4 shows the experimental and model data for $BaTiO_3$ - $Bi(Zn_{1/2}Ti_{1/2})O_3$ (BT-BZT) with a composition of $x = 0.8$. These model results were found using the three polarization components of only three atomic configurations. The model dielectric constant for this composition is slightly lower than experiment for nearly all temperatures, while the actual values are very similar.

B. Non-Zero External Electric Field

So far our discussion and analysis has only included effects from the nearest neighbor interaction term in the Hamiltonian in Equation 1. For ferroelectric materials it helps to understand the behavior of the material in the presence of an external electric field. To include the second term in the Hamiltonian in our analysis, we only need to modify our probability (Eq. 3) to include this new term in the energy:

$$P_{\beta,\vec{E}}(E,\vec{p}) = \frac{\sum_{n=1}^{N} H_n(E,\vec{p}) g_n^{-1} \exp\left(-\beta\left(E - \vec{p}\cdot\vec{E}\right)\right)}{\sum_{m=1}^{N} n_m g_m^{-1} \exp\left(-\beta_m E - f_m\right)} . \quad (16)$$

Note that the energy in the denominator does not include the electric field term, because all simulations were done with zero electric field applied. The beauty of the histogram method is that as long as the polarization and energy microstates exist in the histogram, then the probability of finding the system with that microstate can be found. The energy in the denominator of Equation 16 corresponds to the Hamiltonian used in each simulation. This is made clear since it is this energy that is multiplied by β_m, which corresponds to the simulation temperatures. Since the value of β in the numerator corresponds to the desired temperature, the desired electric field term also makes an appearance. Thus, using the histogram method it is possible to use data simulated at zero applied E-field to get a probability at a non-zero E-field.

The top section of Figure 5 shows the polarization density in the direction of the field as a function of electric field for both the model and experimental data of pure BT at room temperature. The obvious difference between the model and experiment is that the model is completely polarized in the direction of the applied field, even for small fields. Since pure BT is ferroelectric at room temperature, the large polarization is expected, even in the absence of an applied electric field.

The magnitude differs from the experimental values at low fields because the Monte Carlo model predicts a DC

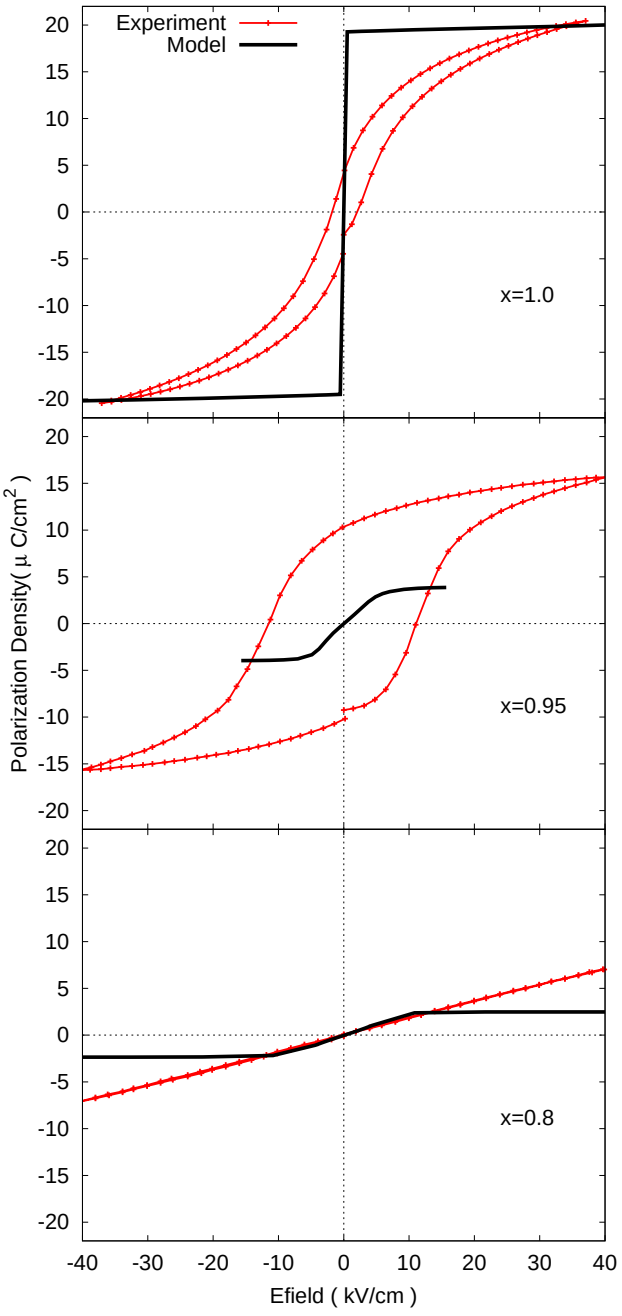

FIG. 5: (color online) Polarization vs electric field for various compositions compared with experiment at room temperature. Experimental data provided by Huang and Cann[25].

value, which corresponds to the infinite time limit of an applied DC field. This leads to the drawback that we are unable to predict the hysteretic behavior shown by experiment. The slope of the polarization versus electric field curve is the susceptibility in the limit of small electric fields. The discontinuity of the predicted curve shows an infinite slope for small fields. This corresponds with the divergence of the dielectric constant below the Curie temperature of BT. In the limit of high field, the experiment and model agree quite nicely. This is due to the fact that high field strengths force the system into a single bulk polarization state that is equivalent to the equilibrium state for the model.

The middle and bottom portions of Figure 5 show the polarization density vs electric field with compositions of 0.95 and 0.8 respectively for both experiment and model data. As was previously stated, and may be more obvious here, the model fails to predict hysteresis, since there can only be one true equilibrium state in the presence of an electric field.

One feature that occurs for both compositions of $x < 1$, is that the maximum polarization of the model is much lower than the maximum for the experiment. This is most likely due to the lack of available microstates with high polarizations in the model. Since the input simulations are all performed with zero applied electric field, the high polarization states most likely have not been sampled. If the solid solutions had high polarization states available as input to the histogram method, the maximum polarization of the $\vec{P}$ vs $\vec{E}$ graphs would better match the experimental values, which suggests that we would benefit from performing additional MC simulations with an applied finite electric field. Even so, the combined multiple histogram method helps us by reducing the number of such simulations required. For BT this issue did not arise because the high polarizations were sampled, since the low temperature states with zero field are identical to states with a large electric field applied.

For all of the solid solution polarization versus electric field graphs there is a finite slope at small applied field, while the slope of the $x = 1$ graph is infinite. The linear behavior of this slope at small applied fields indicates that the materials with lower composition are linear dielectrics, and the value of the slope and the dielectric constant show that they are in fact high permittivity linear dielectrics.

IV. CONCLUSION AND SUMMARY

Using only *ab initio* methods and the experimental Curie temperature of $BaTiO_3$ (BT), we developed a model to predict the dielectric properties of $BaTiO_3$ - $Bi(Zn_{1/2}Ti_{1/2})O_3$ (BT-BZT) in solid solution. This material behaves as a relaxor ferroelectric for some compositions as shown experimentally[25] and through our own predictions.

We first use Density Functional Theory (DFT) to calculate the ground state energies of small $2 \times 2 \times 2$ cubic supercells of the BT-BZT solid solution. This is a slight challenge, since there are many atomic configurations of the solid solution supercells. We then use the Modern Theory of Polarization (MTP) to determine the available polarization states of each supercell. DFT and MTP alone are unable to effectively model relaxors due

to the importance of long range disorder.

In order to model the long-range disorder effects of relaxors we introduce a Monte Carlo lattice Ising-like model, where the cells on the lattice are the supercells used in the DFT calculations with polarization states determined by MTP. Our model differs from Ising, Potts, and Heisenberg models in that each cell has a finite number of polarization states that are of differing magnitude and orientation, and not every cell on the lattice has the same available states. The interaction energy coupling constant needed for this Ising-like model was determined by fitting to the experimental Curie temperature of BT.

To analyze the Monte Carlo data we use the multiple histogram method to combine data from simulations of a single lattice configuration at multiple temperatures. However, to combine simulations of multiple lattice configurations we had to develop a modified version of the multiple histogram method. Using this new analysis tool, we combine Monte Carlo data from multiple simulations and temperatures to obtain the most statistically accurate data possible.

The new model and analysis method allow us to predict a dielectric constant that has reasonable agreement with experiment, especially at high temperatures. The manner in which the predicted dielectric constant as a function of temperature changes with respect to the composition is consistent with that of experiment. We also predict the behavior of the polarization of BT-BZT in the presence of an applied external electric field, with reasonable agreement in the range of small electric fields.

[1] I. K. Jeong, T. W. Darling, J. K. Lee, T. Proffen, R. H. Heffner, J. S. Park, K. S. Hong, W. Dmowski, and T. Egami, Physical review letters **94**, 147602 (2005).

[2] R. Blinc, J. Dolinšek, A. Gregorovič, B. Zalar, C. Filipič, Z. Kutnjak, A. Levstik, and R. Pirc, Physical review letters **83**, 424 (1999).

[3] V. Westphal, W. Kleemann, and M. Glinchuk, Physical review letters **68**, 847 (1992).

[4] J. Hlinka, S. Kamba, J. Petzelt, J. Kulda, C. Randall, and S. Zhang, Physical review letters **91**, 107602 (2003).

[5] P. M. Gehring, S. Wakimoto, Z. G. Ye, and G. Shirane, Physical review letters **87**, 277601 (2001).

[6] V. Bobnar, Z. Kutnjak, R. Pirc, R. Blinc, and A. Levstik, Physical review letters **84**, 5892 (2000).

[7] A. Glazounov and A. Tagantsev, Physical review letters **85**, 2192 (2000).

[8] T. Granzow, T. Woike, M. Wöhlecke, M. Imlau, and W. Kleemann, Physical review letters **89**, 127601 (2002).

[9] S. E. Park and T. R. Shrout, Journal of Applied Physics **82**, 1804 (1997).

[10] G. Burns and F. Dacol, Solid state communications **48**, 853 (1983).

[11] A. Lebon, H. Dammak, and G. Calvarin, Journal of Physics-Condensed Matter **15**, 3069 (2003), ISSN 0953-8984.

[12] G. Y. Xu, Z. Zhong, Y. Bing, Z. G. Ye, and G. Shirane, Nature Materials **5**, 134 (2006), ISSN 1476-1122.

[13] G. A. Samara, Phys. Rev. B **71**, 224108 (2005), URL `http://link.aps.org/doi/10.1103/PhysRevB.71.224108`.

[14] I. Grinberg, Y. H. Shin, and A. M. Rappe, Physical review letters **103**, 197601 (2009).

[15] B. P. Burton, E. Cockayne, and U. V. Waghmare, Physical Review B **72**, 064113 (2005).

[16] S. Tinte, B. P. Burton, E. Cockayne, and U. V. Waghmare, Physical review letters **97**, 137601 (2006).

[17] M. Sepliarsky, S. R. Phillpot, S. K. Streiffer, M. G. Stachiotti, and R. L. Migoni, Applied Physics Letters **79**, 4417 (2001).

[18] B. P. Burton, E. Cockayne, S. Tinte, and U. V. Waghmare, Phase Transitions **79**, 91 (2006), ISSN 0141-1594.

[19] T. Qi, I. Grinberg, and A. M. Rappe, Phys. Rev. B **79**, 094114 (2009), URL `http://link.aps.org/doi/10.1103/PhysRevB.79.094114`.

[20] L. Bellaiche and D. Vanderbilt, Physical review letters **83**, 1347 (1999).

[21] R. Pirc and R. Blinc, Physical Review B **60**, 13470 (1999).

[22] T. Granzow, T. Woike, M. Wöhlecke, M. Imlau, and W. Kleemann, Physical review letters **92**, 65701 (2004).

[23] W. Kleemann, J. Dec, P. Lehnen, R. Blinc, B. Zalar, and R. Pankrath, EPL (Europhysics Letters) **57**, 14 (2002).

[24] X. Duan, W. Luo, W. Wu, and J. S. Yuan, Solid state communications **114**, 597 (2000).

[25] C. C. Huang and D. P. Cann, Journal of Applied Physics **104**, 024117 (2008).

[26] N. Raengthon and D. P. Cann, Ultrasonics, Ferroelectrics and Frequency Control, IEEE Transactions on **58**, 1954 (2011).

[27] X. Wang and A. Yang, Journal of Physics D: Applied Physics **42**, 075419 (2009).

[28] P. G. et. al., Journal of Physics: Condensed Matter **21**, 395502 (19pp) (2009), URL `http://www.quantum-espresso.org`.

[29] R. D. King-Smith and D. Vanderbilt, Physical Review B **47**, 1651 (1993).

[30] D. Vanderbilt and R. D. King-Smith, Physical Review B **48**, 4442 (1993).

[31] R. Resta and D. Vanderbilt, Physics of Ferroelectrics pp. 31–68 (2007).

[32] E. Ising, Zeitschrift für Physik A Hadrons and Nuclei **31**, 253 (1925).

[33] L. Onsager, Physical Review **65**, 117 (1944).

[34] M. H. Jensen and P. Bak, Physical Review B **27**, 6853 (1983).

[35] R. B. Potts, in *Mathematical Proceedings of the Cambridge Philosophical Society* (Cambridge Univ Press, 1952), vol. 48, pp. 106–109.

[36] B. A. Berg, H. Meyer-Ortmanns, and A. Velytsky, Physical Review D **70**, 054505 (2004).

[37] A. Bazavov, B. A. Berg, and S. Dubey, Nuclear Physics B **802**, 421 (2008).

[38] K. Binder, Physical Review Letters **47**, 693 (1981).

[39] A. M. Ferrenberg and R. H. Swendsen, Physical review letters **61**, 2635 (1988).

[40] A. M. Ferrenberg and R. H. Swendsen, Physical Review Letters **63**, 1195 (1989).